

Applications of Minkowski Actions in CAGD
Through Laguerre Geometry

by
Kira Sushkoff
Weiqing Gu, Advisor

Advisor: _____

Second Reader: _____

(Michael E. Orrison)

May 2003

Department of Mathematics

HARVEY MUDD
COLLEGE

Abstract

Applications of Minkowski Actions in CAGD

Through Laguerre Geometry

by Kira Sushkoff

May 2003

Applications of Laguerre geometry to computer aided geometric design are presented, realized through Minkowski actions. Basic Laguerre geometry is first discussed. Then quaternions, set multiplication, and the use of quaternion sets to define Minkowski actions are described and used to achieve results used in geometric design.

Table of Contents

List of Figures	iii
Chapter 1: Introduction	1
1.1 Background	1
1.2 Overview of this Paper	3
Chapter 2: Laguerre Geometry	5
2.1 Standard Model	5
2.2 Cyclographic Model	7
2.3 Cyclographic Mapping	9
Chapter 3: Minkowski Action	17
3.1 Minkowski Product	17
3.2 Minkowski Action of Quaternion Sets	19
Chapter 4: Laguerre Geometry Realized by Minkowski Action	21
4.1 The Cyclographic Mapping	21
4.2 Laguerre Transformations	25
Chapter 5: Offsets	28
5.1 Introduction	28
5.2 Computation of Offsets	28
Chapter 6: Medial Axis Theory	36

6.1	Introduction	36
6.2	The Medial Axis Transform	37
6.3	Conclusion	40
	Bibliography	41

List of Figures

2.1	Hyperbolic line	9
2.2	γ -line	10
2.3	Elliptic line	11
4.1	Cyclographic image of a parabola	23
4.2	Cyclographic image of an ellipse	23
4.3	Cyclographic image of absolute value	24
4.4	Double Cyclide Blend	25
4.5	Dilatation \mathcal{L}_d	26
5.1	Cardioid and offset curves	33
5.2	Ellipsoid and offset surfaces	35
5.3	Hyperboloid and offset surfaces	35
6.1	The Medial Axis Transform	38
6.2	The medial axis of an ellipse	39

Acknowledgments

I would like to thank Professor Weiqing Gu for her infinite patience, assistance and elucidation of difficult mathematical concepts.

Chapter 1

Introduction

1.1 Background

Among the many great mathematical advancements in the nineteenth century were the developments of new ideas of space and new geometries: Lie's sphere geometry, line geometry, and projective and non-Euclidean geometries. The rigid points and parallel lines of Euclid's mathematics became generalized elements of space that could take the form of lines, directed lines, curves, spheres, even coordinate-free or imaginary lines and planes. Geometrical objects transmuted from one form to another, and their relationships to fixed geometric objects were searched for invariant properties. It was in this milieu, in 1853, that French mathematician Edmond Laguerre (1834–1886) first delved into projective geometry [20].

We refer to the classical sphere geometry which resulted from Laguerre's work as *Laguerre geometry*, although extensive results and development of this branch of mathematics were contributed by Klein, Blaschke, Müller, and Krames [24]. Laguerre geometry is based on oriented n -dimensional spheres and planes in oriented contact. The study of oriented contact between these two types of objects was fleshed out by geometers by the 1930s. However, Laguerre geometry is again an exciting area of geometrical research with the recent discovery of its applications to problems in the emerging fields of computer aided geometrical design (CAGD) and computational geometry [16], [19], [21], [24], [25], [30].

Non-Euclidean geometries were not the only new developments in nineteenth

century mathematics by far. Pierpont chronicles the major theories which sprung up during this time period and notes that the single most defining characteristic of mathematics in the nineteenth century is the systematic use of complex numbers and variables [20].

It was in 1813 and 1814 that Argand first published his geometrical interpretation of complex numbers [20]. Hamilton approached complex numbers from the viewpoint of pairs of real numbers and, fascinated with the geometrical implications of this interpretation, searched for 3-dimensional analogues to these ubiquitous new objects. His search culminated in 1843, in his well-known discovery of 4-tuples called quaternions, whose multiplication rules he carved, at the moment of discovery, into the Brougham Bridge in Dublin, Ireland [1]. Hamilton and other algebraists realized that, as the set of complex numbers \mathbb{C} could be thought of as a 2-dimensional vector space over the reals, the set of quaternions \mathbb{H} could be thought of as a 4-dimensional vector space over the reals. *Algebras*—vector spaces like these which possess well-defined multiplication rules for their “basis” vectors—stimulated a trend in the theory of linear spaces toward greater abstraction; the quaternion algebra studied by Hamilton was joined in 1851 by Cayley’s matrix algebras and in 1844 by Grassmann’s peculiar algebras in which elements were not necessarily even specified.

Mathematicians heartily subscribed to the geometrical vector interpretation of complex numbers, and Hamilton and his “quaternionist” followers Tait and Pierce applied a geometrical interpretation to quaternion multiplication to be taken up by Gibbs in his association of sphere rotations to purely imaginary quaternions. Algebras which admit such a geometrical interpretation are called *geometric algebras* and include \mathbb{C} , \mathbb{H} , and Clifford and Grassmann algebras. In 2001, Farouki, Moon and Ravani defined a new geometric algebra, called *Minkowski geometric algebra*, in which the elements were not numbers, but subsets of \mathbb{C} [10]. These sets of complex numbers are interpreted as subsets of the plane and often define polar

curves. In 2002, Gu and Weiner extended Minkowski geometric algebra to include sets of quaternions as the elements and also defined the *Minkowski action* of sets of quaternions [12], giving geometrical intuition throughout.

With the ready geometrical interpretation of quaternion multiplication as rotations in \mathbb{R}^3 , it is no surprise that Shoemake introduced quaternions to CAGD and to the animation of rotations in computer graphics. Shoemake (1985), Pletinckx (1989), Schlag (1991), Barr (1992), Ge and Ravani (1993,1994), Kim and Nam (1995), and others have slowly incorporated quaternions into CAGD research and have begun the integration of quaternion rotational motion and projective geometry in CAGD applications. Both this avenue of research and the Laguerre geometry discussed earlier are promising approaches to the building of mathematical foundations for improved computer-aided design. Hence, following the suggestion in [12], this article utilizes the Minkowski action of quaternions in order to effect Laguerre geometric results and applications to current problems in CAGD.

1.2 Overview of this Paper

In chapter 2, we will describe the basics of Laguerre geometry, discussing both the standard model and what is known as the cyclographic model of Laguerre geometry and giving insight to the connections between them. In chapter 3 we continue the work of the second chapter by finishing the mathematical foundations for chapters 4 through 7. We define quaternions and describe the geometrical interpretation of their multiplication. The notion of multiplication of sets is discussed, and the Minkowski action of quaternion sets is defined.

In chapters 4 through 7, we see transformations and constructions in Laguerre geometry realized as the Minkowski action of one quaternion set on another. We discuss the application of these results to the generation of offset curves and surfaces, which are used in computer-aided milling and machining, and to medial

axis theory, an important tool in the field of computer vision. Finally we discuss results in surface design, paying special attention to the construction and blending of canal surfaces, and the future research on quaternion Minkowski actions to which they point.

Chapter 2

Laguerre Geometry

Like all branches of mathematics, Laguerre geometry studies certain objects and properties which are invariant under specific kinds of transformations. In this case the objects under scrutiny are cycles and hyperplanes, and the transformations which we consider are those mappings which preserve oriented contact between the cycles and oriented hyperplanes.

In Section 2.1 we explain these basic definitions while describing the standard model of Laguerre geometry. In Section 2.2 we present the cyclographic model of Laguerre geometry, which pulls n -dimensional Laguerre geometry into an $n + 1$ -dimensional model. Finally, Section 2.3 explains the cyclographic mapping, which allows us to move between these two models of Laguerre geometry.

2.1 Standard Model

We first present the fundamental definitions of Laguerre geometry.

Definition 1 *An n -dimensional oriented sphere, or **cycle**, is an n -dimensional sphere together with a signed radius.*

Equivalently, a cycle consists of a sphere and an associated unit normal vector field. A radius $r > 0$ indicates an outward normal vector field, a negative radius $r < 0$ indicates an inward normal vector field, and a radius $r = 0$ indicates a point.

We will refer to an n -dimensional cycle with midpoint $m = (m_1, m_2, \dots, m_n)$ and signed radius r as $S^n(m, r)$, denoting the n -dimensional sphere S^n translated to midpoint m and scaled to radius r .

The hyperplane with unit normal vector $\mathbf{e} = (e_1, e_2, \dots, e_n)$ and signed distance e_0 from the origin is described by the equation $e_0 + e_1x_1 + e_2x_2 + \dots + e_nx_n = 0$. The coordinates $[e_0, e_1, e_2, \dots, e_n]$ form an equivalence class of equations describing the same hyperplane, since, for example, $[2e_0, 2e_1, 2e_2, \dots, 2e_n]$ describes the same hyperplane.

Definition 2 *An oriented hyperplane is a hyperplane with an orientation given by a unit normal $\mathbf{e} = (e_1, e_2, \dots, e_n)$. We refer to a hyperplane by its hyperplane coordinates $[e_0, e_1, e_2, \dots, e_n]$.*

Definition 3 *An oriented sphere (cycle) and an oriented hyperplane are in oriented contact if they are tangent and their unit normals coincide at the point of tangency. For a point and an oriented hyperplane, oriented contact equals incidence.*

Special mappings which preserve oriented contact are called Laguerre transformations and are the mappings under consideration in Laguerre geometry. Let \mathcal{C} be the set of cycles in \mathbb{R}^n and \mathcal{E} be the set of oriented hyperplanes in \mathbb{R}^n . Then:

Definition 4 *A Laguerre transformation is a pair of two bijective maps,*

$$\begin{aligned}\mathcal{L} : \mathcal{C} &\rightarrow \mathcal{C} \\ \mathcal{L}^* : \mathcal{E} &\rightarrow \mathcal{E},\end{aligned}\tag{2.1}$$

which preserve oriented contact and noncontact between cycles and oriented hyperplanes.

These mappings are by no means independent; the map \mathcal{L} acts on all cycles of radius 0, which are points. Hence \mathcal{L} acts on each point of an oriented hyperplane to produce an image cycle, and induces the mapping \mathcal{L}^* on \mathcal{E} , which maps each hyperplane to the envelope of its image family of cycles.

Examples of Laguerre transformations include rigid motions, similarities, and, an important class of tools for generating offsets, dilatations.

Definition 5 A dilatation is a Laguerre transformation which adds a constant $d \neq 0$ to the signed radius of each cycle and leaves its midpoint unchanged.

A dilatation is not point preserving; in fact, it maps a point (cycle with $r = 0$) to a cycle with signed nonzero radius d . Each oriented hyperplane is thus mapped to the envelope of the family of oriented cycles generated by points of the hyperplane. We define the image to be the half of the envelope at signed distance d from the original hyperplane, thus preserving oriented contact.

2.2 Cyclographic Model

Another useful way to view n -dimensional Laguerre geometry is to embed \mathbb{R}^n in \mathbb{R}^{n+1} as the hyperplane $x_{n+1} = 0$. Each cycle $S^n(m, r)$ in \mathbb{R}^n , where $m = (m_1, m_2, \dots, m_n)$, is mapped to the point $\zeta(S^n(m, r)) = (m_1, m_2, \dots, m_n, r)$ in \mathbb{R}^{n+1} . With this embedding we also map, via the induced map ζ^* , each oriented n -dimensional hyperplane $[e_0, e_1, \dots, e_n]$ to the $n + 1$ -dimensional hyperplane $\zeta^*([e_0, e_1, \dots, e_n]) = [e_0, e_1, \dots, e_n, 1]$.

A few remarks need to be made considering the pair of mappings ζ, ζ^* . From Section (2.1) we know that the original hyperplane $[e_0, e_1, \dots, e_n]$ is orthogonal distance $|e_0|$ from the origin. Besides containing the original hyperplane, the image hyperplane $[e_0, e_1, \dots, e_n, 1]$ also passes through the point $(0, 0, \dots, 0, -e_0)$, since

$$\begin{aligned} e_0 + e_1 \cdot 0 + e_2 \cdot 0 + \dots + e_n \cdot 0 + 1 \cdot x_{n+1} &= 0 && \text{implies} \\ x_{n+1} &= -e_0. \end{aligned}$$

The Euclidean angle made between the image hyperplane $[e_0, e_1, \dots, e_n, 1]$ and \mathbb{R}^n , thus, equals $\gamma = \tan^{-1}(|-e_0|/|e_0|) = \tan^{-1}(1) = \frac{\pi}{4}$.

Definition 6 A hyperplane in \mathbb{R}^{n+1} which makes a Euclidean angle of $\gamma = \frac{\pi}{4}$ with \mathbb{R}^n is called a γ -hyperplane, and a line in \mathbb{R}^{n+1} which makes a Euclidean angle of $\gamma = \frac{\pi}{4}$ with \mathbb{R}^n is called a γ -line.

Hence, a cycle C is mapped to the point $\zeta(C) \in \mathbb{R}^{n+1}$, and an oriented n -plane E in oriented contact with C in \mathbb{R}^n is mapped by ζ^* to the γ -hyperplane through E and the point $\zeta(C)$. If the cycle C is interpreted as the envelope of a family of oriented n -planes in \mathbb{R}^n , then the image family of $n + 1$ -planes determined by ζ^* has as its envelope a γ -cone whose vertex is $\zeta(C)$ and whose generators are γ -lines. Laguerre transformations in the cyclographic model, then, must map each γ -cone and tangent $n + 1$ -plane pair to another γ -cone and tangent $n + 1$ -plane pair, to preserve oriented contact in the standard model.

2.2.1 Pseudoeuclidean scalar product

In the cyclographic model of Laguerre geometry, since relevant transformations send γ -cones and their tangent hyperplanes to other γ -cone and tangent hyperplane pairs, we use a scalar product which characterizes points as under, on, or above γ -cones as our geometric measure. This scalar product is the *pseudoeuclidean scalar product*.

Definition 7 *The pseudoeuclidean (pe) scalar product of two vectors \mathbf{a} and \mathbf{b} is defined to be*

$$\langle \mathbf{a}, \mathbf{b} \rangle_{pe} := \mathbf{a}^T \cdot E_{pe} \cdot \mathbf{b}, \quad (2.2)$$

where, in \mathbb{R}^{n+1} , E_{pe} is the diagonal matrix with $e_{1,1} = e_{2,2} = \dots = e_{n,n} = 1$, $e_{n+1,n+1} = -1$.

The matrix E_{pe} does not define a metric because it is not positive definite. It does, however, define the quadratic form $x_1^2 + x_2^2 + \dots + x_n^2 - x_{n+1}^2 = 0$. In the most common dimension for application, $n = 2$, this reduces to $x_1^2 + x_2^2 - x_3^2 = 0$, the equation of a γ -cone.

2.3 Cyclographic Mapping

The mapping $c := \zeta^{-1}$ from \mathbb{R}^{n+1} to \mathbb{R}^n maps the point $x = (x_1, x_2, \dots, x_n, x_{n+1})$ to the cycle $c(x)$ in \mathbb{R}^n with center $m = (x_1, x_2, \dots, x_n)$ and radius $r = x_{n+1}$. The mapping $c^* := \zeta^{*-1}$ maps the γ -hyperplane E in \mathbb{R}^{n+1} to the oriented n -plane ζ^{*-1} which is the intersection of E and \mathbb{R}^n .

Definition 8 The pair of mappings $(c, c^*) : \mathbb{R}^{n+1} \rightarrow \mathbb{R}^n$ is called the cyclographic mapping.

2.3.1 Cyclographic image of a line

A simple line in \mathbb{R}^{n+1} will have a different image under the cyclographic mapping depending on the Euclidean angle which it makes with \mathbb{R}^n .

Example 2.1 For a vector $\mathbf{a} \in \mathbb{R}^3$, if $\langle \mathbf{a}, \mathbf{a} \rangle_{pe} > 0$, then a line with direction \mathbf{a} makes an angle $\gamma < \frac{\pi}{4}$ with \mathbb{R}^2 and is called a hyperbolic line. Its cyclographic image, the envelope of the family of image cycles of its points, consists of two oriented lines.

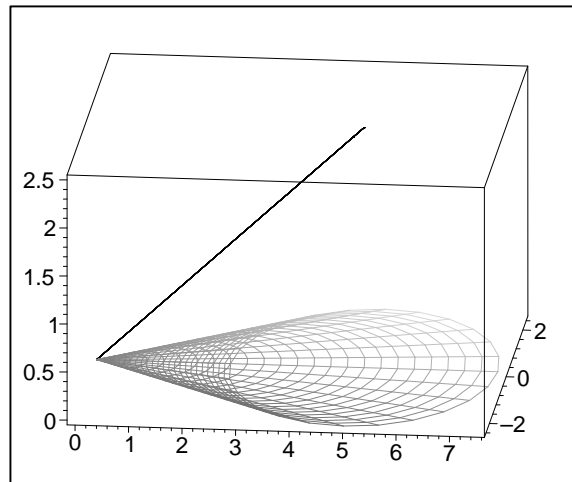


Figure 2.1: A hyperbolic line and its cyclographic image

Example 2.2 A vector $\mathbf{a} \in \mathbb{R}^3$ which has $\langle \mathbf{a}, \mathbf{a} \rangle_{pe} = 0$ makes the angle $\gamma = \frac{\pi}{4}$ with \mathbb{R}^2 and, hence, a line with direction \mathbf{a} is a γ -line, or a parabolic line. The image cycles of such a line are all tangent to one line, so the envelope of this family of cycles, its cyclographic image, is just that one single oriented line in \mathbb{R}^2 .

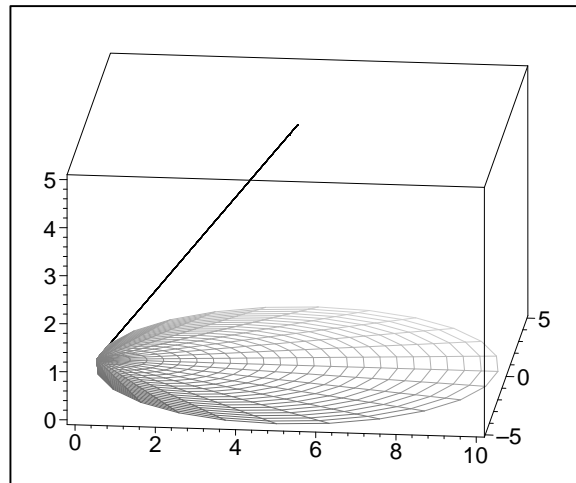


Figure 2.2: A γ -line and its cyclographic image

Example 2.3 If $\langle \mathbf{a}, \mathbf{a} \rangle_{pe} < 0$ for $\mathbf{a} \in \mathbb{R}^3$, then a line with direction \mathbf{a} makes an angle $\gamma > \frac{\pi}{4}$ with \mathbb{R}^2 and is called elliptic. Its family of image cycles covers \mathbb{R}^2 , so it has no envelope, hence an imaginary cyclographic image.

Definition 9 Consider two points a and b in \mathbb{R}^{n+1} . The pseudoeuclidean (pe) distance of a and b is defined to be $d = \sqrt{\langle a - b, a - b \rangle_{pe}}$.

Let $a = c^{-1}(A)$ and $b = c^{-1}(B)$ be two points in \mathbb{R}^3 . Then any common tangent oriented line of the two cycles A and B in \mathbb{R}^2 touches A and B at points with Euclidean distance d , called the *tangential distance* of A and B .

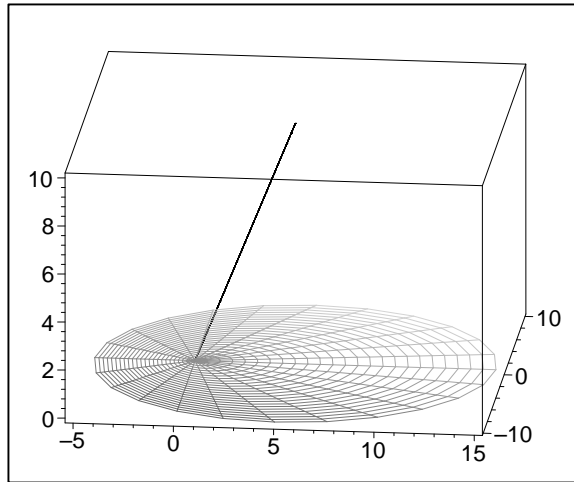


Figure 2.3: An elliptic line and its cyclographic image

Theorem 2.3.1 Consider two points $a = c^{-1}(A)$ and $b = c^{-1}(B)$ in \mathbb{R}^3 . Then the tangential distance d of A and B in \mathbb{R}^2 equals the square root of the pe distance of a and b in \mathbb{R}^3 (where this is real and defined):

$$d = \sqrt{\langle b - a, b - a \rangle_{pe}}. \quad (2.3)$$

Proof : Let $a = (m_1, m_2, r)$, let $b = (M_1, M_2, R)$, and let E be the line through a and b . Let γ be the angle which E makes with \mathbb{R}^2 , where γ is arbitrary. Then the vertical distance between a and b is $R - r$, while the distance between (m_1, m_2) and (M_1, M_2) is $\sqrt{(M_1 - m_1)^2 + (M_2 - m_2)^2}$. Thus,

$$\tan \gamma = (R - r) / \sqrt{(M_1 - m_1)^2 + (M_2 - m_2)^2}. \quad (2.4)$$

So

$$\begin{aligned} \sqrt{\langle b - a, b - a \rangle_{pe}} &= \left(\langle (M_1 - m_1, M_2 - m_2, R - r), (M_1 - m_1, M_2 - m_2, R - r) \rangle_{pe} \right)^{1/2} \\ &= \left((M_1 - m_1)^2 + (M_2 - m_2)^2 - (R - r)^2 \right)^{1/2} \\ &= \sqrt{(1 - \tan^2 \gamma) \left((M_1 - m_1)^2 + (M_2 - m_2)^2 \right)} \quad \text{by (2.4)}. \end{aligned} \quad (2.5)$$

But since height of a point in \mathbb{R}^3 equals radius of its cyclographic image, the same right triangle used above is formed in \mathbb{R}^2 with sides d and $R - r$ and hypotenuse $\sqrt{(M_1 - m_1)^2 + (M_2 - m_2)^2}$, so that, similarly,

$$d = \sqrt{(1 - \tan^2 \gamma) ((M_1 - m_1)^2 + (M_2 - m_2)^2)}.$$

Thus, $d = \sqrt{\langle b - a, b - a \rangle_{pe}}$. ■

We use this theorem to prove the above claims about cyclographic images of lines.

- If a and b lie on a hyperbolic line, i.e. $0 \leq \gamma < \frac{\pi}{4}$, then $\tan \gamma < 1$, so by equation 2.5, d is positive and A and B possess two common tangent lines.
- If a and b lie on a γ -line, then $\tan \gamma = 1$, so by equation 2.5, $d = 0$ and A and B coincide at their one point of tangency.
- If a and b lie on an elliptic line, i.e. $\frac{\pi}{4} < \gamma \leq \pi$, then $\tan \gamma > 1$, so by equation 2.5, d is imaginary, so the cyclographic image of the elliptic line is imaginary; A and B possess no common tangent lines.

The pe metric naturally lends itself to the description of Laguerre transformations, and the following two theorems from [24] demonstrate this utility.

Theorem 2.3.2 *There is a 1-1 correspondence between pe congruences in \mathbb{R}^{n+1} and tangential distance-preserving Laguerre transformations in \mathbb{R}^n .*

Theorem 2.3.3 *All Laguerre transformations are pseudoeuclidean (pe) similarities*

$$x' = a + \lambda A \cdot x, \tag{2.6}$$

where a is a translation factor, λ is a scaling factor, and A is a pseudoeuclidean orthogonal matrix.

2.3.2 Cyclographic Mapping of Curves

Now that we have described the cyclographic mapping of lines, we can use oriented *line elements* to describe the cyclographic image of curves. We say *line element*, denoted (x, l) , to describe the point x along with a small direction Δs given by the direction of oriented line l . Let $p(t)$ be C^1 a curve in \mathbb{R}^3 . For each $x \in p$, we consider the line element $(x, x + \lambda p')$, where $x + \lambda p'$ is the line through $x = p(t_0)$ in the direction of the tangent vector $p'(t_0)$.

From section 2.3.1, we know that if the tangent vector $p'(t_0)$ makes the angle γ with \mathbb{R}^2 , then the cyclographic image of $(x, x + \lambda p')$ is one oriented line element (x_1, t_1) . In this case, x_1 is the intersection of $x + \lambda p'$ and \mathbb{R}^2 , and t_1 is the oriented line in contact with $c(x)$ at x_1 . The γ -plane through $x + \lambda p'$, whose normal has x_1, x_2 -direction given by the projection of p' onto \mathbb{R}^2 , intersects \mathbb{R}^2 in the line t_1 .

For a hyperbolic tangent vector $p'(t_0)$, the cyclographic image of $(x, x + \lambda p')$ is two oriented line elements (x_1, t_1) and (x_2, t_2) , where t_1 and t_2 are the intersections with \mathbb{R}^2 of the two γ -planes through the tangent line $x + \lambda p'(t_0)$. The points x_1 and x_2 then are the intersections of the cycle $c(x)$ with oriented lines t_1 and t_2 , respectively. An elliptic line element has no real image.

To map the curve $p(t)$ we map the line element $(p, p + \lambda p')$ for each point along the curve. By definition, $c(p)$ is the envelope of the image oriented line elements.

The simplest case occurs when all the tangents to a curve $p \in \mathbb{R}^3$ make the angle γ with \mathbb{R}^2 . We call these curves γ -curves. Another way to find $c(p)$ of a γ -curve is to consider the surface

$$T(p)(t, \lambda) = p(t) + \lambda p'(t). \quad (2.7)$$

$T(p)$ is a developable surface, as we can easily show. A surface $X(t, \lambda) = \alpha(t) + \lambda w(t)$ is said to be *developable* if

$$(w, w', \alpha') \triangleq (w \wedge w') \cdot \alpha' \triangleq \det(w, w', \alpha') \equiv 0.$$

Thus, for $T(p)$, $\alpha = p$ and $w = p'$. Then

$$\begin{aligned}
 \det(w, w', \alpha') &= \det(p', p'', p') \\
 &= -\det(p', p', p'') \\
 &= -(p' \wedge p') \cdot p'' \\
 &\equiv 0.
 \end{aligned} \tag{2.8}$$

The tangent planes of $T(p)$ (osculating planes of p) form the constant angle γ with \mathbb{R}^2 , hence we call $T(p)$ a γ -developable. The usefulness of considering $T(p)$ appears in the following theorem.

Theorem 2.3.4 *Let $p(t) \subset \mathbb{R}^3$ be a γ -curve. Its cyclographic image $c(p)$ is $T(p) \cap \mathbb{R}^2$, the intersection of $T(p)$ with \mathbb{R}^2 .*

Proof : For ease of calculation we assume p lies entirely in the upper half space of \mathbb{R}^3 . The situation simply reverses orientation when a curve crosses into the negative half-space and thus $r < 0$. By definition,

$$\begin{aligned}
 T(p) &= p(t) + \lambda p'(t) \\
 &= (p_1(t) + \lambda p'_1(t), p_2(t) + \lambda p'_2(t), p_3(t) + \lambda p'_3(t)).
 \end{aligned} \tag{2.9}$$

To find $T(p) \cap \mathbb{R}^2$, we solve $p_3(t) + \lambda p'_3(t) = 0$. Hence $\lambda = -\frac{p_3(t)}{p'_3(t)}$. So

$$T(p) \cap \mathbb{R}^2 = \left(p_1 - \frac{p_3 p'_1}{p'_3}, p_2 - \frac{p_3 p'_2}{p'_3} \right).$$

Now we calculate the cyclographic image $c(p)$. Let $x = (p_1, p_2, p_3) = p(t_0)$ be a point of p and let $(x, x + \lambda p'(t_0))$ be the associated line element. Let (x_1, t_1) denote the cyclographic image line element of $(x, x + \lambda p')$. Then $c(x)$ is a cycle with center (p_1, p_2) and radius $p_3 > 0$. So x_1 is the point on $c(x)$ in the opposite direction of p' :

$$x_1 = (p_1, p_2) - p_3 \frac{(p'_1, p'_2)}{\|(p'_1, p'_2)\|}. \tag{2.10}$$

Now p' is a γ -vector, so $\langle p', p' \rangle_{pe} \equiv 0$, i.e. $p_1'^2 + p_2'^2 - p_3'^2 \equiv 0$. Thus,

$$\begin{aligned} c(p) &= (p_1, p_2) - p_3 \frac{(p_1', p_2')}{(p_3'^2)^{1/2}} \\ &= \left(p_1 - \frac{p_3 p_1'}{p_3'}, p_2 - \frac{p_3 p_2'}{p_3'} \right). \end{aligned} \tag{2.11}$$

$\therefore T(p) \cap \mathbb{R}^2 = c(p)$. ■

The proof of this fact gives several more results concerning the cyclographic image of a γ -curve. Let $p \in \mathbb{R}^3$ be a C^1 γ -curve parameterized by arc length. We can assume this because it is always possible to find a curve $q(t)$ parameterized by arc length which has the same trace as $p(t)$ [4]. Then $\|p'(t)\| \equiv 1$ and $p''(t) = k(t)n(t)$, where $k(t)$ is the curvature of $p(t)$ and $n(t)$ is the unit normal to $p(t)$.

Definition 10 *The evolute of a curve $\alpha(t) \subset \mathbb{R}^2$ is given by $\beta(t) = \alpha(t) + \frac{1}{k(t)}n(t)$, where $k(t)$ is the curvature of $\alpha(t)$ and $n(t)$ is the unit normal to $\alpha(t)$.*

We then have the following results for γ -curves:

- The orthogonal projection onto \mathbb{R}^2 of a γ -curve p parameterized by arc length is the evolute of $c(p)$.
- The term p_3^{-1} gives the curvature of $c(p)$.
- The vector $\left(\frac{p_1'}{p_3'}, \frac{p_2'}{p_3'}\right)$ gives the unit normal to $c(p)$.

For an arbitrary C^1 curve $p \in \mathbb{R}^3$, the γ -developable through p is more difficult to describe. The definition of $T(p)$ is more general than the γ -curve case, in which $T(p)$ is ruled by the tangent lines of p . Let $\tau(t)$ be the family of γ -planes through the tangent lines $x + \lambda p'$ of p . We described the direction of these γ -planes on page 13. Parabolic tangents have one γ -plane through them, hyperbolic tangents have

two γ -planes through them, and elliptic tangents have none. Then the envelope of the family $\tau(t)$ forms $T(p)$, which we call the γ -developable through p .

For arbitrary $C^1 p \subset \mathbb{R}^3$, we still have the fact $c(p) = T(p) \cap \mathbb{R}^2$. We show this in section 5.2, where we generalize the results on $T(p)$ for γ -curves in \mathbb{R}^3 to arbitrary C^1 curves in \mathbb{R}^3 .

Pottman and Peternell summarize in [24] some facts about the cyclographic image $c(p)$ of curves in $p \in \mathbb{R}^3$ which are important for applications of 2-dimensional Laguerre geometry. Some of these results are:

- Let t_0 be an isolated root of the function defined by $\langle p'(t), p'(t) \rangle_{pe}$. In this case, $\langle p'(t), p'(t) \rangle$ undergoes a sign change at t_0 , so that the point $p(t_0)$ separates an elliptic segment of the curve p from a hyperbolic segment of p . Then the point $c(p(t_0))$ is a *vertex* of the image curve $c(p)$.
- Let t_0 be an inflection point of $p(t)$. Then the curve $c(p)$ has an inflection point at $p(t_0)$. The image curve $c(p)$ has in fact two inflection points at $p(t_0)$ when $p'(t_0)$ is hyperbolic.
- Let t_0 be an isolated root of the function defined by $p_3(t)$. Then $p(t_0)$ is a double point of $c(p)$, that is, the point $c(p(t_0))$ is traced out twice by $c(p)$.

Having thus built a foundation of the Laguerre geometry of \mathbb{R}^2 and \mathbb{R}^3 , we now turn to the geometric algebra which will describe the associated 3- and 4-dimensional cyclographic models: the Minkowski geometric algebra of quaternion sets.

Chapter 3

Minkowski Action

In Section 3.1 we describe the geometric interpretation of quaternion multiplication, with the identification of \mathbb{R}^3 and $\mathbf{i}, \mathbf{j}, \mathbf{k}$ -space, since they are isomorphic as vector spaces. In Section 3.2 we describe the Minkowski product, a notion of multiplying whole sets of quaternions instead of singleton quaternions. We then discuss the Minkowski action of one quaternion set on another, which is an extension of the Minkowski product.

3.1 Minkowski Product

3.1.1 Quaternion Multiplication

Recall that the set of quaternions, \mathbb{H} , is a normed division algebra with elements of the form $a1 + b\mathbf{i} + c\mathbf{j} + d\mathbf{k}$, for $a, b, c, d \in \mathbb{R}$, where multiplication is defined by

1.) 1 is the multiplicative identity

$$2.) \quad \mathbf{i}^2 = \mathbf{j}^2 = \mathbf{k}^2 = -1$$

$$3.) \quad \mathbf{ij} = \mathbf{k}; \quad \mathbf{ji} = -\mathbf{k}$$

$$\mathbf{jk} = \mathbf{i}; \quad \mathbf{kj} = -\mathbf{i}$$

$$\mathbf{ki} = \mathbf{j}; \quad \mathbf{ik} = -\mathbf{j}$$

We identify \mathbb{H} with \mathbb{R}^4 so that the x_1 -axis is the \mathbf{i} -axis, the x_2 -axis is the \mathbf{j} -axis, the x_3 -axis is the \mathbf{k} -axis, (which comprises \mathbb{R}^3), and the fourth axis, the x_4 -axis, is identified with the scalar axis. In this way, totally imaginary quaternions become vectors in \mathbb{R}^3 .

3.1.2 Geometric Interpretation

Using the multiplication rules above, [12] and [31] show that given a unit length quaternion

$$\mathbf{p}_0 = \cos \theta + \mathbf{u}_{p_0} \sin \theta, \quad (3.1)$$

left multiplication $\mathbf{p}_0\mathbf{q}$ of an arbitrary quaternion $\mathbf{q} \in \mathbb{H}$ by \mathbf{p}_0 effects a 4-dimensional rotation of \mathbf{q} as follows:

- The plane spanned by 1 and \mathbf{u}_{p_0} is rotated counterclockwise by θ . The counterclockwise direction in this plane brings 1 toward \mathbf{u}_{p_0} .
- The plane in $\mathbf{i}, \mathbf{j}, \mathbf{k}$ -space that is orthogonal to the first plane, which we shall call the $\mathbf{u}_{p_0}^\perp$ plane, is also rotated counterclockwise by angle θ . The counterclockwise direction in the $\mathbf{u}_{p_0}^\perp$ plane is determined by the “right hand rule” while pointing one’s thumb in the direction of \mathbf{u}_{p_0} .

Right multiplication $\mathbf{q}\mathbf{p}_0$ by a unit quaternion \mathbf{p}_0 has a similar effect: the plane spanned by $\{1, \mathbf{u}_{p_0}\}$ is again rotated counterclockwise by θ , but the $\mathbf{u}_{p_0}^\perp$ plane is now rotated *clockwise* by θ .

Thus, left and right multiplication by unit quaternions can be coupled to effect purely 3-dimensional rotations. In particular, if we replace θ with $-\theta$, \mathbf{p}_0 is replaced by its conjugate

$$\bar{\mathbf{p}}_0 = \cos \theta - \mathbf{u}_{p_0} \sin \theta.$$

Then, left multiplication by \mathbf{p}_0 and right multiplication by $\bar{\mathbf{p}}_0$ counteract each other in the $1, \mathbf{u}_{p_0}$ -plane and double the angle of rotation in the $\mathbf{u}_{p_0}^\perp$ plane. Gu and Weiner show in [12] that for an arbitrary quaternion $\mathbf{q} \in \mathbb{H}$, conjugation by \mathbf{p}_0 effects a rotation of the imaginary part of \mathbf{q} in $\mathbf{i}, \mathbf{j}, \mathbf{k}$ -space about the axis \mathbf{u}_{p_0} . Specifically, the imaginary part of \mathbf{q} is rotated counterclockwise in the $\mathbf{u}_{p_0}^\perp$ plane by an angle 2θ while the real part of \mathbf{q} is held fixed.

As a consequence of these geometric interpretations, any 3-dimensional rotation of vectors in i, j, k -space can be accomplished by conjugation by a unit quaternion, which is unique up to sign. And, any 4-dimensional rotation can be achieved by left and right multiplication by unit quaternions, which are uniquely determined up to sign [12].

3.2 Minkowski Action of Quaternion Sets

Now that we know the geometric interpretation of singleton quaternion multiplication, we describe the geometry of multiplication of quaternion sets. The Minkowski product defines multiplication of sets of quaternions and is a higher-dimensional analog of interval arithmetic.

Definition 11 *Given quaternion sets $\mathcal{A}, \mathcal{B} \in \mathbb{H}$, we define the Minkowski product of \mathcal{A} and \mathcal{B} to be*

$$\mathcal{A} \otimes \mathcal{B} = \{\mathbf{ab} \mid \mathbf{a} \in \mathcal{A} \text{ and } \mathbf{b} \in \mathcal{B}\}.$$

This definition is motivated by the analogous definition of Minkowski product of complex sets defined and explored in [10]. Similarly, a set addition can be defined on quaternion sets.

Definition 12 *Given quaternion sets $\mathcal{A}, \mathcal{B} \in \mathbb{H}$, we define the Minkowski sum of \mathcal{A} and \mathcal{B} to be*

$$\mathcal{A} \oplus \mathcal{B} = \{\mathbf{a} + \mathbf{b} \mid \mathbf{a} \in \mathcal{A} \text{ and } \mathbf{b} \in \mathcal{B}\}.$$

Gu and Weiner show in [12] that these operations do indeed form an algebra, hence called Minkowski geometric algebra. Using these definitions we can achieve surfaces and regions in both two and three dimensions as the product or sum of simpler quaternion curves. (The case of 2-dimensional curves reduces to the Minkowski geometric algebra of complex curves explored in [9], [10], [11], and [14].) A more advantageous definition would utilize both Minkowski sums and

products of quaternion sets to define and describe geometrical constructs. This motivates the definition of the Minkowski action.

Definition 13 Let $\mathcal{A} \subset \mathbb{R} \times \mathbb{H}^3$ and $\mathcal{X} \subset \mathbb{H}$. We define $\mathcal{A}(\mathcal{X}) \subset \mathbb{H}$ by

$$\mathcal{A}(\mathcal{X}) = \{a_s \mathbf{a}_l \mathbf{x} \bar{\mathbf{a}}_r + \mathbf{a}_\tau \mid (a_s, \mathbf{a}_l, \mathbf{a}_r, \mathbf{a}_\tau) \in \mathcal{A}\}$$

We call this set the action of \mathcal{A} on \mathcal{X} .

In practice, we take \mathbf{a}_l and \mathbf{a}_r to be unit quaternions, so that a_s can be a true scaling factor. Then, each point $\mathbf{x} \in \mathcal{X}$ is rotated through left multiplication by \mathbf{a}_l and right multiplication by \mathbf{a}_r , as described in Section 3.1. If we choose $\mathbf{a}_r = \mathbf{a}_l^{-1}$, then the imaginary part of \mathbf{x} is rotated in 3-space as described also in Section 3.1. The resultant point is then scaled by the scaling factor a_s and translated by the translating factor \mathbf{a}_τ . In this way, the Minkowski action of one quaternion set on another prescribes the construction of a subset of \mathbb{R}^4 , and taking only the imaginary “coordinates” produces a subset of \mathbb{R}^3 , as we see in the next chapter.

Chapter 4

Laguerre Geometry Realized by Minkowski Action

In this chapter, we show that many of the operations performed in Laguerre geometry can be written naturally as the Minkowski action of one quaternion set on another. Usually these operations will be achieved by the action of a quaternion curve in n dimensions on another set. An immediate advantage of this technique is the ease with which we generalize results on 2-dimensional Laguerre geometry for 3-dimensional Laguerre geometry.

4.1 The Cyclographic Mapping

For applications in computer aided geometrical design, the cyclographic mapping has only been used as applied to curves in \mathbb{R}^{n+1} , where $n = 2, 3$. It is very convenient, thus, that given a curve $p(t) = (m_1(t), m_2(t), \dots, m_n(t), r(t))$ in \mathbb{R}^4 or \mathbb{R}^3 , for t in some interval I , we can easily realize the cyclographic mapping applied to $p(t)$ by letting an appropriate set act on S^2 or S^1 , respectively.

4.1.1 Images of Curves in \mathbb{R}^3

Let $p(t) = (m_1(t), m_2(t), r(t))$ in \mathbb{R}^3 , for t in some interval I . We identify \mathbb{R}^3 with $\mathbf{i}, \mathbf{j}, \mathbf{k}$ -space so that \mathbb{R}^2 is identified with \mathbf{i}, \mathbf{j} -space. Then the cyclographic image of $p(t)$ consists of the envelope of S^1 scaled by $r(t)$ and translated by $\mathbf{m}(t) = m_1(t)\mathbf{i} + m_2(t)\mathbf{j}$. We parameterize S^1 by

$$\begin{aligned} S^1 &= \{e^{k\theta}\mathbf{i} \mid 0 \leq \theta \leq 2\pi\} \\ &= \{\cos(\theta)\mathbf{i} + \sin(\theta)\mathbf{j} \mid 0 \leq \theta \leq 2\pi\}. \end{aligned}$$

Then

$$\mathcal{A} = \{(r(t), 1, 1, \mathbf{m}(t) \mid t \in I\} \quad \text{for interval } I \text{ under consideration,}$$

and we have

$$\begin{aligned} c(p(t)) &= \mathcal{A}(S^1) \\ &= \{r\mathbf{q} + \mathbf{m} \mid \mathbf{q} \in S^1, (r, 1, 1, \mathbf{m}) \in \mathcal{A}\}. \end{aligned}$$

For application in CAGD, we can instead parameterize S^1 using its rational parametrization. Then if the component curves in $\mathcal{A}(t)$ are rational, $\mathcal{A}(S^1)$ defines a rational curve, which can thus be represented in current computer-aided design or computer-aided machining systems.

In Figure 4.1, a segment of a parameterized parabola acts on S^1 to produce the image in \mathbb{R}^2 . Recall from section 2.3.2 that the cyclographic image of an isolated root of $\langle p'(t), p'(t) \rangle_{pe}$ produces a vertex in the cyclographic image curve (see page 16). In Figure 4.1 we highlighted two such points which separate the hyperbolic segment of the parabola (black) from the elliptic portions of the parabola (grey). The cyclographic images of the curve segments with elliptic tangent vectors (grey) are imaginary and hence are not shown.

In Figure 4.2, a parameterized ellipse acts on S^1 to produce the image in \mathbb{R}^2 . If p is an ellipse or hyperbola in \mathbb{R}^3 which is symmetric to \mathbb{R}^2 , then the cyclographic image of p is a conic section with focal points at the intersections of p and \mathbb{R}^2 [24].

For another example, the piecewise continuous absolute value function acts on S^1 to produce the image in Figure 4.3.

4.1.2 Images of Curves in \mathbb{R}^4

Slight modification of this technique allows us to realize surfaces in \mathbb{R}^3 as the cyclographic image of curves in \mathbb{R}^4 . For simplification, we identify $\mathbf{i}, \mathbf{j}, \mathbf{k}$ -space with

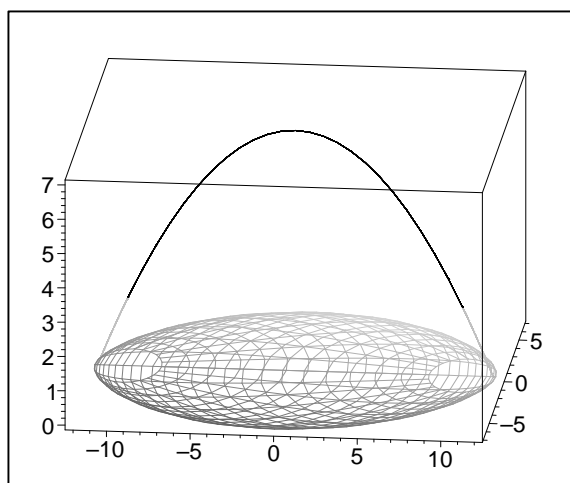


Figure 4.1: Cyclographic mapping of a normal parabola in \mathbb{R}^3

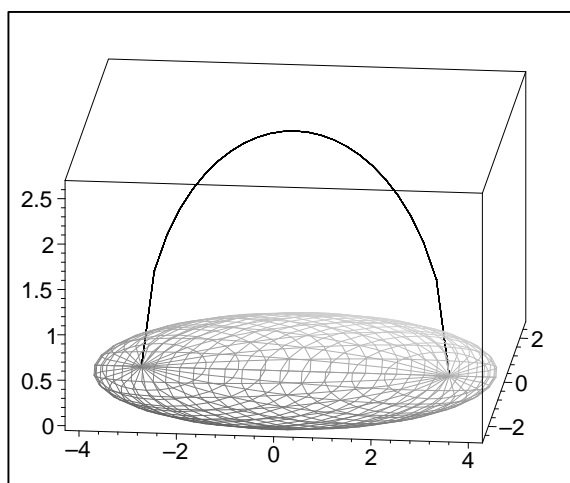


Figure 4.2: Cyclographic mapping of an ellipse p in \mathbb{R}^3 symmetric with respect to \mathbb{R}^2 . p intersects \mathbb{R}^2 at the foci of the image ellipse.

\mathbb{R}^3 . We parameterize S^2 as

$$S^2 = (\sin \varphi \cos \theta, \sin \varphi \sin \theta, \cos \varphi) = \sin \varphi \cos \theta \mathbf{i} + \sin \varphi \sin \theta \mathbf{j} + \cos \varphi \mathbf{k}.$$

Let $p(t) = (m_1(t), m_2(t), m_3(t), r(t))$ in \mathbb{R}^4 , for t in some interval I . We still scale

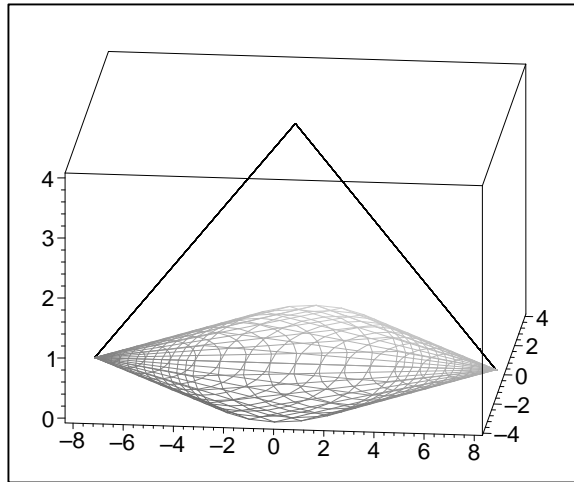


Figure 4.3: Cyclographic mapping of the absolute value function in \mathbb{R}^3

S^2 by $r(t)$, but now we translate by $\mathbf{m}(t) = m_1(t)\mathbf{i} + m_2(t)\mathbf{j} + m_3(t)\mathbf{k}$. Then

$$\mathcal{A} = \{(r(t), 1, 1, \mathbf{m}(t) \mid t \in I\} \quad \text{for interval } I \text{ under consideration,}$$

and we have

$$\begin{aligned} c(p(t)) &= \mathcal{A}(S^2) \\ &= \{r\mathbf{q} + \mathbf{m} \mid \mathbf{q} \in S^2, (r, 1, 1, \mathbf{m}) \in \mathcal{A}\}. \end{aligned} \quad (4.1)$$

A pipe surface, which is a surface traced out by spheres of constant radius with centers lying on some space curve $p \subset \mathbb{R}^3$, always admits a rational parametrization if its *spine curve* p is rational. Pottmann and Lü prove this fact and give an algorithm for its construction in [15]. We can generate a wider class of rational surfaces, including pipe surfaces, in the example above by instead parameterizing S^2 using its rational parametrization. $\mathcal{A}(S^2)$ then gives a rational surface if the component curves of $\mathcal{A}(t)$ are rational, for compatibility with computer-aided design systems. Only rational surfaces can be represented authentically in current CAD systems; other surfaces must be approximated by rational surfaces called NURBS

(Non-Uniform Rational B-Spline) surfaces, in order to be represented in current CAD.

Canal surfaces, pipe surfaces of spheres with varying radius, can be constructed by using the action described in equation 4.1. Additionally, we can let arcs of the specific curves in \mathbb{R}^4 called pe circles act on S^2 to produce *Dupin cyclides*, which are canal surfaces used to blend cones and cylinders together [16], [24]. Given two cones in space, it is generally the case that one Dupin cyclide cannot blend the first cone smoothly into the second. Hence we use pairs of Dupin cyclides spliced together by the spline consisting of the corresponding pairs of pe arcs in \mathbb{R}^4 , in order to smoothly blend arbitrary cones. Such pairs of Dupin cyclides are called *double cyclide blends*.

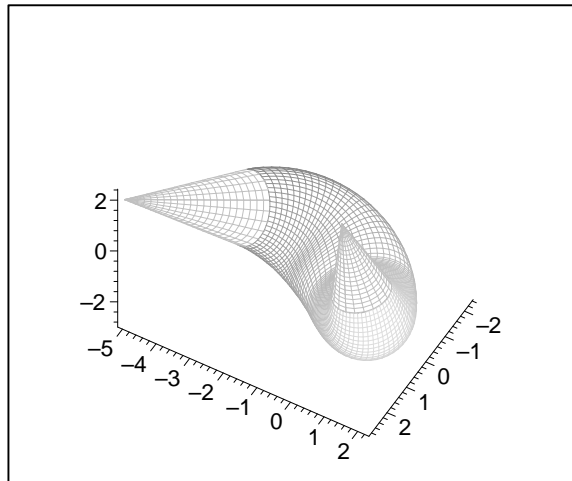


Figure 4.4: A double cyclide blend with minimal radial variation connects two cones with skew axes.

4.2 Laguerre Transformations

Throughout its wide applications, the standard model of Laguerre geometry in \mathbb{R}^n is most useful in the cases $n = 2$ and $n = 3$. For the $n = 2$ case, cycles and oriented

hyperplanes become 2-dimensional sets and thus are represented as subsets of a 2-dimensional subspace of \mathbb{H} , which we can identify with \mathbb{C} . The commutative nature of the objects we study allows us this identification because two quaternions commute if and only if there exists a plane containing both of them and the real axis [12], and every 2-plane in \mathbb{H} that contains the real axis is ring-isomorphic to \mathbb{C} [12]. However, for easier generalization and for consistency of notation, we work in the 2-dimensional \mathbf{i}, \mathbf{j} -plane in the following examples.

4.2.1 Dilatation

Recall from Section 2.1 that a dilatation, \mathcal{L}_d , is a Laguerre transformation which adds a constant $d \neq 0$ to the signed radius of each cycle and leaves its midpoint unchanged. In \mathbb{R}^2 , \mathcal{L}_d maps a curve to its offset curve at a perpendicular distance of $|d|$, and the sign of d determines whether this distance is taken parallel (negative) or antiparallel (positive) to the normal vector of the curve defined by its orientation.

We denote a cycle with center $\mathbf{m} = m_1\mathbf{i} + m_2\mathbf{j}$ and radius r (possibly 0) as $S^1(m, r)$. Let the dilatation $\mathcal{L}_d : (\mathcal{C}, \mathcal{E}) \rightarrow (\mathcal{C}, \mathcal{E})$ be defined by

$$\mathcal{L}_d : S^1(m, r) \mapsto S^1(m, r + d).$$

Then \mathcal{L}_d maps line $l(\mathbf{e})$ with normal \mathbf{e} in oriented contact with $S^1(m, r)$ to the line $l(\mathbf{E})$ with normal \mathbf{E} in oriented contact with $S^1(m, r + d)$.

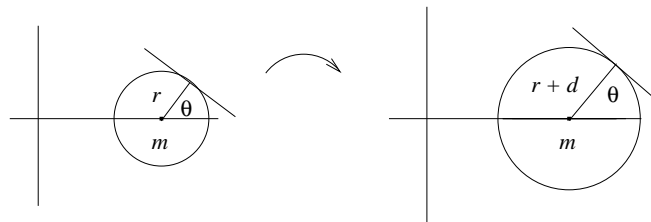


Figure 4.5: Dilatation \mathcal{L}_d

Write $S^1(m, r)$ and $l(\mathbf{e})$ as parameterized sets of quaternion numbers in the \mathbf{i}, \mathbf{j} -plane

$$\begin{aligned} \mathbf{z} &= \{r e^{k\theta} \mathbf{i} + \mathbf{m} \mid 0 \leq \theta \leq 2\pi\} \\ \mathbf{w} &= \{(r e^{k\theta_0} \mathbf{i} + \mathbf{m}) + t(e^{k(\theta_0 + \frac{\pi}{2})}) \mathbf{i} \mid t \in I\}, \end{aligned} \tag{4.2}$$

respectively. Then the map \mathcal{L}_d can be realized as the action of the singleton point $\mathcal{A} = \left\{ \left(\frac{r+d}{r}, 1, 1, -\left(\frac{r+d}{r} \right) \mathbf{m} + \mathbf{m} \right) \right\}$ on the set of quaternions $\mathbf{z} \cup \mathbf{w}$.

Chapter 5

Offsets

5.1 Introduction

Offset curves and surfaces and curves and surfaces at a constant distance λ from a given curve or surface. For example, the interior of a ship or automobile may be described as an offset surface of the exterior at distance λ given by the thickness of the material. Offset curves are used in decorative designs but also also play an important role in computer-aided machining (CAM), especially in the form of offset space curves. They describe tool paths for milling pockets or holes in objects, for example in the milling of dies and molds used to make automobile parts [13]. During 3-axis NC (Numerically Controlled) milling of a free form surface, a reference point on the axis of the cutting tool has to move on an offset surface in order to have accurate shape control and collision prevention. When you use a ball cutter (versus cylindrical, toroidal and many other shapes of cutters), that reference point moves on a *general offset surface*, which is the surface wished to be milled, displaced by a constant multiple of its unit normal vector [23]. Computation of offset surfaces is thus essential for tool path planning in surface milling.

5.2 Computation of Offsets

In this section, we utilize results from the cyclographic model of Laguerre geometry to compute offsets of curves and surfaces in 2 and 3 dimensions. Since offsets are effectively the loci of points with constant distance to a given curve or surface, we find our first useful fact in the following theorem.

Theorem 5.2.1 *The γ -developable $T(p)$ to an arbitrary C^1 curve $p \in \mathbb{R}^3$ is the graph of the signed distance function to $c(p) \in \mathbb{R}^2$.*

Proof : Let $(x, x + \lambda p')$ be a tangent line element to curve p . For elliptic $(x, x + \lambda p')$, there is no image line element. For parabolic or hyperbolic $(x, x + \lambda p')$, let (x_1, t_1) be an image line element of $(x, x + \lambda p')$.

In order for oriented contact to occur between the cycle $c(x)$ and the oriented line t_1 , the unit normal to t_1 at x_1 must coincide with the unit normal to $c(x)$ at x_1 , which is the unit normal to the envelope $c(p)$ at x_1 . The projection onto \mathbb{R}^2 of the line from x to x_1 is always orthogonal to (x_1, t_1) , and hence, normal to the curve $c(p)$ at x_1 . The distance between a point and a curve is measured along the normal direction, if that direction can be defined. Thus, points $y = (y_1, y_2)$ lying on the projection of the xx_1 line will have distance $|y - x_1|$ to $c(p)$, with positive (negative) sign when $y - x_1$ is antiparallel (parallel) to the normal to $c(p)$.

Project y along a ray parallel to $(0, 0, 1)$ until the line (y_1, y_2, t) first intersects $T(p)$ in (y_1, y_2, y_3) . Then since $T(p)$ is a γ -developable, the signed distance $y - x_1$ from y to x_1 in \mathbb{R}^2 equals the vertical distance from y to x_1 , which is $y_3 - 0 = y_3$. Hence the signed distance to $c(p)$ is y_3 , which is the height of $T(p)$ at (y_1, y_2) . ■

Notice that Theorem 5.2.1 implies that the intersection of $T(p)$ and \mathbb{R}^2 has zero distance to $c(p)$, hence $c(p) = T(p) \cap \mathbb{R}^2$ for arbitrary C^1 curves in \mathbb{R}^3 . We use this fact to compute offset curves in this chapter and later, in Chapter 6, to compute the medial axes of 2-dimensional shapes.

5.2.1 Offset Curves

An oriented, possibly closed curve $c \subset \mathbb{R}^2$ can be thought of as the cyclographic image of a curve $p \subset \mathbb{R}^3$. We then use Theorem 5.2.1 to find offset curves to c .

Let $c(t)$ be a smooth curve in \mathbb{R}^2 . We consider first the case c is a simple closed curve or not closed at all, where c is the cyclographic image of a curve $p \subset \mathbb{R}^3$.

Assume without loss of generality that the pre-image curve p lies in the upper half-space of \mathbb{R}^3 , so that $r \geq 0$ always. Recall that $r > 0$ is equivalent to a clockwise orientation of c or, for a closed curve, an outward normal. To construct an offset curve we want to move the curve along the direction determined by its normal, which we do by rotating the tangent c' clockwise by $\frac{\pi}{2}$ radians and translating the curve by the resultant vector.

For each point $c(t)$, the ruling through $c(t)$ of the γ -developable $T(p)$ is in the direction determined by the normal to c , since $T(p)$ is the graph of the signed distance function to c (Theorem 5.2.1). We identify \mathbb{R}^3 with $\mathbf{i}, \mathbf{j}, \mathbf{k}$ -space so that \mathbb{R}^2 is identified with \mathbf{i}, \mathbf{j} -space. Assume that $c(t)$ is parameterized by arc length and write $c = (c_1, c_2)$ as $\mathbf{c} = c_1\mathbf{i} + c_2\mathbf{j}$. We then can write c' as the quaternion $\mathbf{c}' = c'_1\mathbf{i} + c'_2\mathbf{j}$ and consider the quaternion curve $\mathbf{c}'(t)$. We rotate \mathbf{c}' clockwise by $\frac{\pi}{2}$ radians by multiplying by \mathbf{k} on the right and effecting a 4-dimensional rotation. Notice that multiplication by \mathbf{k} on the right induces a clockwise rotation by $\frac{\pi}{2}$ radians in the \mathbf{i}, \mathbf{j} -plane but also a counterclockwise rotation by $\frac{\pi}{2}$ radians in the $1, \mathbf{k}$ -plane. In dealing with planar curves, we restrict ourselves to the \mathbf{i}, \mathbf{j} -plane, so the rotation of the $1, \mathbf{k}$ -plane does not affect us. When dealing with all of \mathbb{R}^3 , however, we must use quaternion conjugation instead of quaternion multiplication to effect purely 3-dimensional rotations.

If we define the set $\mathcal{A} \subset \mathbb{R} \times \mathbb{H}^3$ to be

$$\mathcal{A}(\lambda, t) = \{(\lambda, 1, \mathbf{k}, \mathbf{c}(t) + \lambda\mathbf{k}) \mid t \in I, \lambda \in J\}, \quad (5.1)$$

then the Minkowski action of \mathcal{A} on \mathbf{c}' gives the γ -developable $T(p)$ through $p(t)$. If $c(t)$ is not parameterized by arc length, then we scale \mathbf{c}' by $\|\mathbf{c}'\|^{-1}$ to retain the angle γ made with \mathbb{R}^2 . Our acting set thus becomes:

$$A = \left\{ \left(\frac{\lambda}{\|\mathbf{c}'(t)\|}, 1, \mathbf{k}, \mathbf{c}(t) + \lambda\mathbf{k} \right) \mid t \in I, \lambda \in J \right\}. \quad (5.2)$$

Since a curve can always be parameterized by arc length, it is theoretically sufficient to consider only the formulation 5.1.

Then for $\gamma \equiv \text{constant}$, $\mathcal{A}(c')$ gives curves in \mathbb{R}^2 at a constant signed distance λ to c , which we call the *untrimmed offsets to c* at signed distance λ . These correspond to level curves of $T(p)$, or horizontal slices of $T(p)$ at height λ which are then projected onto \mathbb{R}^2 . An untrimmed offset can have self-intersections and segments which are not distance λ from c , which must be trimmed off to form the *trimmed offset to c* . Points which must be trimmed have, as their projection pre-images, coordinates (y_1, y_2, λ) where there exists $0 < h < \lambda$ (or $\lambda < h < 0$) such that (y_1, y_2, h) is a self-intersection point of $T(p)$.

Trimming is an important modification of offset curves for their applications in design. When used as decorative designs on boats, woodwork and the like, untrimmed offsets are decidedly aesthetically displeasing. When used in computer-aided NC (Numerically Controlled) milling, the segments of untrimmed offsets which do not have the desired minimal distance to c represent unwanted collisions between the milling tool cutter and the milled material. Another important modification of offsets is the inclusion of curve segments to deal with cusps and corners in the original curve c .

Definition 14 Let $c(t_0)$ be a point of the piecewise smooth curve $c(t) \subset \mathbb{R}^2$ such that $\lim_{t \rightarrow t_0^-} c'(t) = t^-$ and $\lim_{t \rightarrow t_0^+} c'(t) = t^+$ exist, but that

$$\lim_{t \rightarrow t_0^-} c'(t) \neq \lim_{t \rightarrow t_0^+} c'(t).$$

Then $c(t)$ has a tangent discontinuity at t_0 .

At points of tangent discontinuity, we fill in the gap between the two tangents t^- and t^+ with coincident base point by introducing a 1-parameter family of lines through $c(t_0)$ which interpolates t^- and t^+ by rotating through the smallest angle θ between t^- and t^+ . Letting our acting set \mathcal{A} act on these lines adds a portion of a γ -cone to the γ -developable $T(p)$. Only when $\theta < 0$ does the additional arc projected from horizontal slices of the γ -cone contribute to the trimmed offset curve.

Definition 15 Let $c(t_0)$ be a point of the piecewise smooth curve $c(t) \subset \mathbb{R}^2$ such that $c(t_0)$ is not a tangent discontinuity and such that $\lim_{t \rightarrow t_0^-} c''(t)$ and $\lim_{t \rightarrow t_0^+} c''(t)$ exist, but that

$$\lim_{t \rightarrow t_0^-} c''(t) \neq \lim_{t \rightarrow t_0^+} c''(t).$$

Then $c(t)$ has a curvature discontinuity at t_0 .

Curvature discontinuities occur, for example, where an arc smoothly joins a straight line segment in a plane curve c . Unlike tangent discontinuities, curvature discontinuities present no problem to computing offsets. To compute the offsets to more general piecewise smooth curves, we apply the same principle, using the acting set \mathcal{A} and adding portions of γ -cones at discontinuities when needed. The last case occurs when c is closed but not simple, as in a trace of the figure eight. In this case, offsets in the bounded domains formed by c change in their sign of λ after intersection points of c . Taking level curves of the γ -developable with opposite-signed heights for each simple closed piece of c , we can construct the offsets to the original curve.

A cardioid is an example of a closed curve with a tangent discontinuity. At the origin, the two tangent vectors differ by a rotation of π radians. Thus, in addition to the γ -developable through its cyclographic pre-image curve, we add half, i.e. π radians, of a γ -cone centered at the origin before taking level curves of the γ -developable. Trimming occurs after points of intersection of the surface and γ -cone and after points of self-intersection.

We can also compute offsets to C^1 space curves $p \subset \mathbb{R}^3$. These offsets take the form of pipe surfaces with spine curve p . A simple action, via translation, of $p(t)$ on S^2 scaled with radius λ produces these offset surfaces, as shown in more detail in section 4.1.

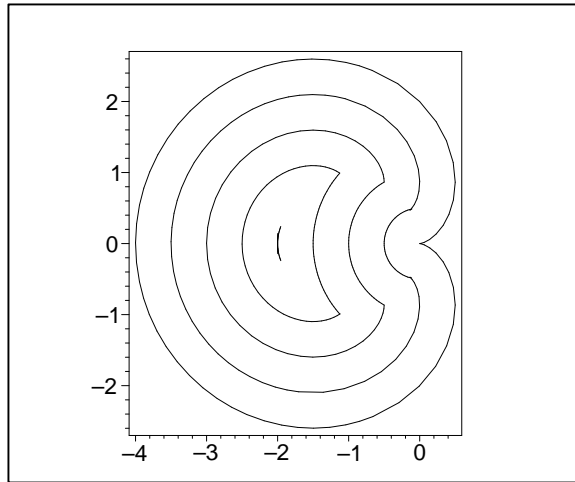


Figure 5.1: A cardioid and some of its trimmed offset curves

5.2.2 Offset Surfaces

A generalization of the method we used for construction of offset curves is given for surfaces in \mathbb{R}^3 , and in this section, we outline the modifications necessary to construct offset surfaces.

Let $X(u, v)$ be a regular surface in \mathbb{R}^3 , that is, a surface which we are able to cover with a family of diffeomorphisms from \mathbb{R}^2 onto subsets of X such that a nonzero normal to X is locally defined for each point $p \in X$. One way in which we might generate offset surfaces to X is by considering X as the cyclographic image of a curve $p(t) \subset \mathbb{R}^4$, and by constructing the γ -developable through p by considering the tangent vector $p'(t)$, as in the case of constructing offset curves.

Another way in which we might generate offset surfaces of X is by displacing the surface by a multiple of the surface normal. We choose arbitrarily to act on $\mathbf{X}_u(u, v)$. Thus, we want to rotate \mathbf{X}_u through an angle of $\frac{\pi}{2}$ radians in the plane spanned by \mathbf{X}_u and $\mathbf{X}_u \wedge \mathbf{X}_v$. Now that we have three dimensions under consideration, we use quaternion conjugation to effect 3-dimensional rota-

tions. Since we know that conjugation by a unit quaternion written in polar form $\mathbf{p}_0 = \cos(\theta) + \mathbf{u}_{p_0} \sin(\theta)$ rotates the $\mathbf{u}_{p_0}^\perp$ plane counterclockwise by angle 2θ , we seek \mathbf{p}_0 such that the $\mathbf{u}_{p_0}^\perp$ plane is the $\mathbf{X}_u, \mathbf{X}_u \wedge \mathbf{X}_v$ -plane.

Thus, if we define the set $\mathcal{A} \subset \mathbb{R} \times \mathbb{H}^3$ to be

$$\mathcal{A}(\lambda, u, v) = \{(\lambda, \mathbf{p}_0, \bar{\mathbf{p}}_0, \mathbf{X}(u, v) + \lambda) \mid u \in I_u, v \in I_v, \lambda \in J\}, \quad (5.3)$$

where $\mathbf{p}_0 = \frac{1}{\sqrt{2}} + \frac{1}{\sqrt{2}}\mathbf{u}_{p_0}$ and the $\mathbf{u}_{p_0}^\perp$ plane is the $\mathbf{X}_u, \mathbf{X}_u \wedge \mathbf{X}_v$ -plane, then the Minkowski action of \mathcal{A} on \mathbf{X}_u gives the graph of the signed distance function to X , and for $\gamma \equiv \text{constant}$, $\mathcal{A}(\mathbf{X}_u)$ gives surfaces in \mathbb{R}^3 at a constant signed distance λ to X , the *untrimmed offset surfaces to X* at signed distance λ . Each of these corresponds to the intersection $\mathcal{A}(\mathbf{X}_u) \cap E$ of the γ -developable $\mathcal{A}(\mathbf{X}_u)$ with 3-dimensional hyperplane E parallel to \mathbb{R}^3 , which is then projected onto \mathbb{R}^3 . Untrimmed offsets can again have self-intersections and pieces which are not distance λ from X , which must be trimmed off to form the trimmed offset surfaces to X . Pieces which need to be trimmed off have, as their projection pre-images, coordinates (x_1, x_2, x_3, λ) where there exists $0 < h < \lambda$ (or $\lambda < h < 0$) such that (x_1, x_2, x_3, h) is a self-intersection point of $\mathcal{A}(\mathbf{X}_u)$.

Some suitably symmetric surfaces have offset surfaces which do not intersect and hence need no trimming. Two examples of these types of surfaces are the surfaces of revolution below. A sphere and some of its offsets are shown in Figure 5.2, and a hyperboloid of one sheet is shown with some of its offsets in Figure 5.3.

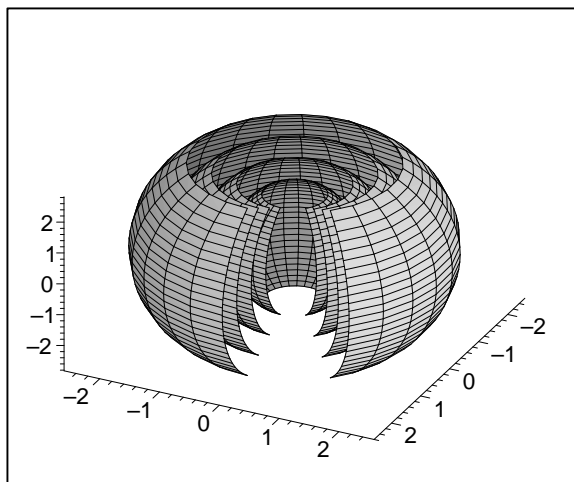


Figure 5.2: An ellipsoid and some of its offset surfaces

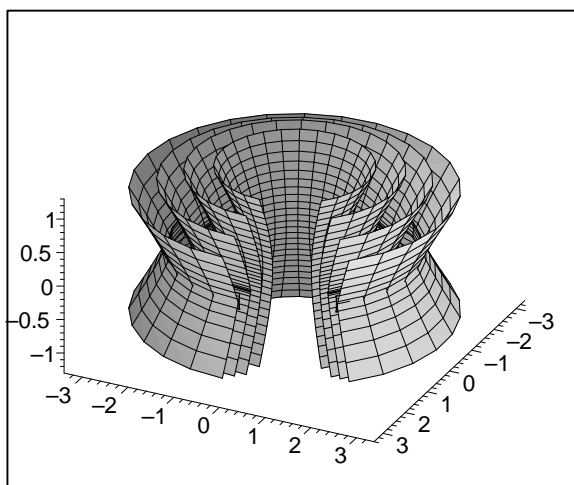


Figure 5.3: A hyperboloid and some of its offset surfaces

Chapter 6

Medial Axis Theory

6.1 Introduction

The concept of medial axis is a close cousin to the offset. Whereas an offset is the curve or surface at a *constant* distance to a given curve or surface, a medial axis is a kind of “skeleton” of a given shape, such that each point of the skeleton is equidistant from at least two points on the boundary of the shape. Since medial axes thus represent shapes in an intuitive and concise manner, they are one of the most influencing constructs in computer vision today [5]. In fact, medial axes are not only used in computer vision and robot vision, but also in the subfields of CAD including pattern analysis, feature extraction and shape recognition, image compression, tool path planning for NC (Numerically Controlled) milling machines, computer graphics, surface fitting and FEM (Finite Element Meshing) [5], [26],[29]. Mathematically, we formulate the medial axis as follows.

Definition 16 *Let Ω be a bounded domain in \mathbb{R}^2 or \mathbb{R}^3 . The medial axis of Ω is the locus of centers of the maximally inscribed circles within Ω which touch the boundary $\partial\Omega$ in at least 2 points.*

The medial axis defines a kind of symmetry for the given domain, which is why we require contact at at least two points.

Definition 17 *A circle is a maximally inscribed circle of bounded domain Ω if its interior $C \subset \Omega$ satisfies the following properties:*

- *C belongs to the set S of the open disks that do not have any points of $\partial\Omega$*

- C is not a proper subset of any other open disk in S .

6.2 The Medial Axis Transform

One of the two basic problems in medial axis theory is: given a medial axis, how do we reconstruct the image which it represents? The answer is given by a “width” function for the skeleton represented by the medial axis called the *medial axis transform* (MAT).

Definition 18 Let Ω be a bounded domain in \mathbb{R}^2 or \mathbb{R}^3 . The medial axis transform of Ω , denoted $\text{MAT}(\Omega)$, is the set of the pairs consisting of the center and the radius of the maximal inscribed circles of Ω .

Notice that the MAT of a domain $\Omega \subset \mathbb{R}^2$ has x_3 -coordinates given by the radii of the maximally inscribed circles. Thus, the projection of the medial axis transform for a domain $\Omega \subset \mathbb{R}^2$ onto \mathbb{R}^2 gives the medial axis of Ω .

6.2.1 From MAT To Shape

Given the medial axis transform $p(t) = (m_1(t), m_2(t), r(t))$ in \mathbb{R}^3 , $t \in I$, for the boundary $\partial\Omega$ of a closed domain Ω in \mathbb{R}^2 , we let the set

$$\mathcal{A} = \{(r(t), 1, 1, \mathbf{m}(t)) \mid t \in I\},$$

where $\mathbf{m}(t) = m_1(t)\mathbf{i} + m_2(t)\mathbf{j}$, act on $S^1 = \{e^{k\theta}\mathbf{i} \mid 0 \leq \theta \leq 2\pi\}$. Then $\mathcal{A}(S^1)$ recreates the domain Ω in \mathbb{R}^2 via the cyclographic map.

An analogous notion of medial axis and medial axis transform can be defined for closed surfaces in \mathbb{R}^3 . Let the medial axis transform of a closed surface $\partial\Omega$, bounding a connected region Ω in \mathbb{R}^3 , be the 4-dimensional curve segment $p(t) = (m_1(t), m_2(t), m_3(t), r(t)) \in \mathbb{R}^4$ for $t \in I$. We recreate the closed surface $\partial\Omega$ which it represents by letting the set

$$\mathcal{A} = \{(r(t), 1, 1, \mathbf{m}(t)) \mid t \in I\},$$

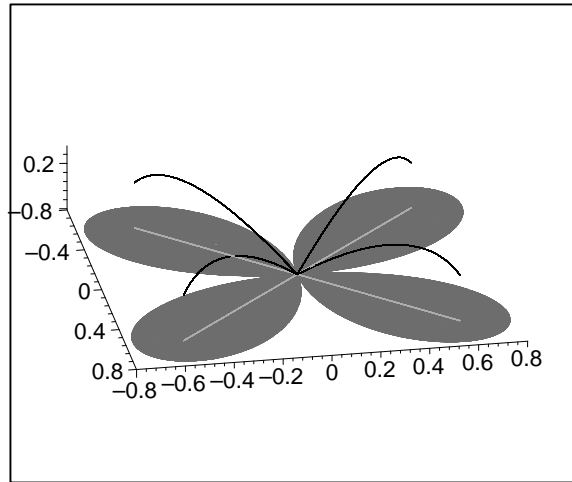


Figure 6.1: The MAT for the four-leaved rose is shown in black, with the rose beneath it in dark grey. The projected medial axis is shown in light grey.

where $\mathbf{m}(t) = m_1(t)\mathbf{i} + m_2(t)\mathbf{j} + m_3(t)\mathbf{k}$, act on S^2 . $\mathcal{A}(S^2)$ then reproduces the surface $\partial\Omega$ in \mathbb{R}^3 .

6.2.2 From Shape to Medial Axis

The second basic problem in medial axis theory is: given a 2-dimensional or 3-dimensional domain, what is its medial axis, and furthermore, what is its medial axis transform? We consider the case of a 2-dimensional domain first. In forming the medial axis transform from a closed curve c , we first must construct a γ -developable. A boundary of a domain Ω in \mathbb{R}^2 may be thought of as the cyclographic image of a curve $p \in \mathbb{R}^3$. Recall from Section 5.2 that the γ -developable $T(p)$ is the graph of the signed distance function to $c(p)$. Thus, arguments similar to the proof of Theorem 2.3.4 can be used to show that the cyclographic image c of a general C^1 curve $p \subset \mathbb{R}^3$ is given by $T(p) \cap \mathbb{R}^2$. The projection of p onto \mathbb{R}^2 is still the evolute of c . Thinking of $\partial\Omega$ as the cyclographic image of a curve p in \mathbb{R}^3 , the MAT of Ω is simply the pre-image curve of $\partial\Omega$.

For domains with smooth boundaries, the medial axis is then given by self-intersection points of $T(p)$ whose projections onto \mathbb{R}^2 lie within Ω . As is the case in constructing offset curves, we add parts of γ -cones at tangent discontinuities of $\partial\Omega$. Then segments of the intersection curves of these γ -cones and $T(p)$ comprise prongs of the MAT when their projections onto \mathbb{R}^2 lie within Ω . These projections form prongs of the medial axis of Ω .

There are three types of “prongs”, or terminating segments of the trimmed medial axis: the maximally inscribed disks can have two points of tangency as their limit approaches a point (a triangle), the maximally inscribed disks can terminate in one minimal osculating circle with one tangency (and osculating) point, or the maximally inscribed disks can terminate in one osculating circle with an arc of contact (a symmetrical construct of two straight line segments joined smoothly to an arc of a circle) [3].

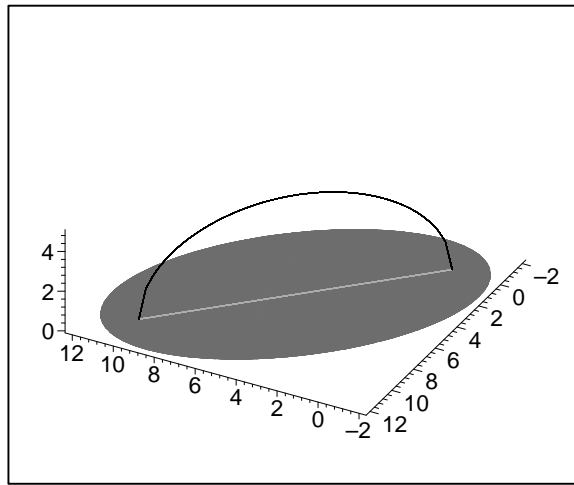


Figure 6.2: The medial axis of an ellipse is shown in light grey. The MAT for this ellipse is graphed in black in \mathbb{R}^3 and intersects \mathbb{R}^2 at the terminal points of the medial axis.

In Section 5.2 we proved results for smooth curves in \mathbb{R}^2 . In general, however, requiring that the boundary curve $\partial\Omega$ be smooth, or C^∞ , is not sufficient for a well-

behaved or even well-defined medial axis. Many examples of bounded domains with C^∞ boundaries and pathological medial axes are described in [2]. The medial axis for such a curve can have infinitely many prongs emanating from one point, or can have infinitely many branches. Thus, for meaningful consideration of medial axes, we restrict the boundary curves we consider to piecewise continuous curves with curve segments comprised of a finite number of real analytic pieces.

Unfortunately, the computation of medial axes amounts to the computation of surface self-intersections, a nontrivial computational problem which we presently possess no robust algorithms for solving. One area of future research, thus, is to examine how we can apply the Minkowski action to the problem of surface intersection computations.

6.3 Conclusion

Minkowski actions of quaternion sets were used to generate many constructs in Laguerre geometry which apply to current problems in computer aided design. However, this investigation was based heavily on 2-dimensional Laguerre geometry and was only extended to 3-dimensional Laguerre geometry and analogous problems in Chapters 4 and 5. Additional work should examine further properties of the Minkowski action, analogous to the studies of Minkowski geometric algebra of complex sets in [9],[10], [11],[14], and will extend results to 3-dimensional problems in CAD.

Bibliography

- [1] John C. Baez. The Octonions. *Bulletin of the American Mathematical Society*, pages 1–61, 2001.
- [2] H. Choi, S. Choi, and H. Moon. Mathematical theory of medial axis transform. *Pacific J. Math.*, 181(1):57–88, 1997.
- [3] S. Choi and H. Seidel. Linear one-sided stability of mat for weakly injective domain, June 2001.
- [4] Manfredo P. do Carmo. *Differential Geometry of Curves and Surfaces*. Prentice-Hall, London, 1976.
- [5] R. Fabbri, L.F. Estrozi, and L. F. Costa. On voronoi diagrams and medial axes. *Journal of Mathematical Imaging and Vision*, 17(1):27–40, July 2002.
- [6] Gerald Farin. *Curves and Surfaces for CAGD: A Practical Guide, Fifth Edition*. Academic Press, London, 2002.
- [7] R. T. Farouki and V. T. Rajan. Algorithms for polynomials in Bernstein form. *Comput. Aided Geom. Design*, 5(1):1–26, 1988.
- [8] Rida T. Farouki. Computing with barycentric polynomials. *Math. Intelligencer*, 13(4):61–69, 1991.
- [9] Rida T. Farouki, Hwan Pyo Moon, and Bahram Ravani. Algorithms for Minkowski products and implicitly-defined complex sets. *Adv. Comput. Math.*, 13(3):199–229, 2000.

- [10] Rida T. Farouki, Hwan Pyo Moon, and Bahram Ravani. Minkowski geometric algebra of complex sets. *Geom. Dedicata*, 85(1-3):283–315, 2001.
- [11] Rida T. Farouki and Helmut Pottmann. Exact Minkowski products of N complex disks. *Reliab. Comput.*, 8(1):43–66, 2002.
- [12] Weiqing Gu and Ian Weiner. Minkowski geometric algebra of quaternion sets. *International Journal of Pure and Applied Mathematics*, 3(4):385–411, 2002.
- [13] Josef Hoschek, Dieter Lasser, and Larry L. Schumaker. *Fundamentals of computer aided geometric design*. A. K. Peters, Ltd., 1993.
- [14] Anil Kaul and Rida T. Farouki. Computing Minkowski sums of plane curves. *Internat. J. Comput. Geom. Appl.*, 5(4):413–432, 1995.
- [15] Wei L and Helmut Pottmann. Pipe surfaces with rational spine curve are rational. *Computer Aided Geometric Design*, 13(7):621–628, 1996.
- [16] Martin Peternell. Sphere geometry with applications. In *SIAM Short Course on Applications of Classical Geometry in CAD*, Albuquerque, November 6 1999.
- [17] Martin Peternell and Helmut Pottmann. Designing rational surfaces with rational offsets. In *Advanced topics in multivariate approximation (Montecatini Terme, 1995)*, volume 8 of *Ser. Approx. Decompos.*, pages 275–286. World Sci. Publishing, River Edge, NJ, 1996.
- [18] Martin Peternell and Helmut Pottmann. Computing rational parametrizations of canal surfaces. *J. Symbolic Comput.*, 23(2-3):255–266, 1997. Parametric algebraic curves and applications (Albuquerque, NM, 1995).
- [19] Martin Peternell and Helmut Pottmann. A Laguerre geometric approach to rational offsets. *Comput. Aided Geom. Design*, 15(3):223–249, 1998.

- [20] James Pierpont. The history of mathematics in the nineteenth century. *Bulletin of the American Mathematical Society*, 37(1):9–24, 1999.
- [21] H. Pottmann, W. Lu, and B. Ravani. Rational ruled surfaces and their offsets. *GMIP*, 58(6):544–552, November 1996.
- [22] Helmut Pottmann. Rational curves and surfaces with rational offsets. *Comput. Aided Geom. Design*, 12(2):175–192, 1995.
- [23] Helmut Pottmann. General offset surfaces. *Neural Parallel Sci. Comput.*, 5(1-2):55–79, 1997. Computer aided geometric design.
- [24] Helmut Pottmann and Martin Peternell. Applications of Laguerre geometry in CAGD. *Comput. Aided Geom. Design*, 15(2):165–186, 1998.
- [25] Helmut Pottmann and Johannes Wallner. *Computational line geometry*. Mathematics+Visualization. Springer-Verlag, Berlin, 2001.
- [26] R. Ramamurthy and R. T. Farouki. Voronoi diagram and medial axis algorithm for planar domains with curved boundaries i. theoretical foundations. *Journal of Computational and Applied Mathematics*, 102(1):119–141, February 1999.
- [27] R. Ramamurthy and R.T. Farouki. Voronoi diagram and medial axis algorithm for planar domains with curved boundaries – ii: Detailed algorithm description. *Journal of Computational and Applied Mathematics*, 102(2):253–277, February 1999.
- [28] Doron Shaked and Alfred M. Bruckstein. Pruning medial axes. *Computer Vision and Image Understanding*, 69(2):156–169, 1998.

- [29] Ralph Costa Teixeira. *Curvature Motions, Medial Axes and Distance Transforms*. PhD thesis, Harvard University, Cambridge, Massachusetts, June 1998.
- [30] Johannes Wallner, Horng-Yang Chen, and Helmut Pottmann. Galilei Laguerre geometry and rational circular offset surfaces. *Beiträge Algebra Geom.*, 39(2):291–305, 1998.
- [31] J. P. Ward. *Quaternions and Cayley Numbers*. Kluwer, Dordrecht, 1997.